

Seismic design and evaluation of a minimal-damage steel frame equipped with steel yielding devices and viscous dampers



T.L. Karavasilis & A.I. Dimopoulos

School of Engineering, University of Warwick, Coventry, UK

E. Hale

Engineering Consultancy, Mott McDonald, UK

SUMMARY:

This paper evaluates an alternative seismic design approach for steel structures that concentrates damage in easy-to-replace steel energy dissipation devices and protects the main structural members from yielding with capacity design rules. This approach is further enhanced by using rate-dependent dampers in parallel to steel devices to achieve drift reduction and protection of drift-sensitive non-structural elements. A model for steel energy dissipation devices is proposed and calibrated against experimental results. The model can accurately predict the experimentally obtained hysteresis and is implemented in the OpenSees software for use in seismic response analysis. A prototype steel building equipped with steel devices and viscous dampers is designed according to explicitly defined minimal-damage performance objectives. Seismic analyses results indicate that the building is able to achieve immediate occupancy under the design seismic action and rapid return to occupancy under the maximum considered seismic action.

Keywords: Hysteretic model, Steel frames, Passive energy dissipation, Performance-based seismic design

1. INTRODUCTION

The European seismic code EC8 (2004) covers conventional lateral-load resisting systems, such as steel moment-resisting frames (MRFs), designed to experience inelastic deformations in main structural members (beams, columns or braces) under strong earthquakes. These inelastic deformations result in difficult-to-repair damage and downtime during which the building is repaired and cannot be used or occupied. To overcome these problems, an alternative seismic design strategy that concentrates damage in removable steel yielding devices and protects the rest of the structural system from yielding is highlighted. This design strategy is further enhanced by using viscous dampers in parallel to the steel yielding devices.

A model for steel yielding devices exhibiting non-degrading hysteretic behavior, such as slit steel devices (Chan and Albermani 2008), low-strength steel shear panels (Nakashima 1995) and buckling restrained braces (BRBs) (Merritt et al. 2003) is proposed. The Bouc-Wen model (Wen 1976) is modified to simulate combined kinematic and isotropic hardening and is calibrated against existing experimental results. The model can accurately predict the experimentally obtained hysteresis and is implemented in the OpenSees software (Mazzoni et al. 2006) for use in seismic response analysis of buildings with steel yielding devices.

A prototype steel building is designed according to EC8 and EC3 (2005) following the proposed seismic design strategy. The results of seismic analyses show that the building achieves immediate occupancy (IO) under the design seismic action (DBE) and rapid return to occupancy (RRO) under the maximum considered seismic action (MCE).

2. PROPOSED MODEL FOR STEEL YIELDING DEVICES

The standard Bouc-Wen model results from the parallel combination of an elastic component and an elastic-perfectly plastic component. The force output F of the model is

$$F = pku + (1 - p)F_y z \quad (2.1)$$

where u is the deformation across the model, F_y the yield force, k the elastic stiffness, p the post-yield stiffness ratio, and z a dimensionless hysteretic parameter governed by

$$\dot{z} = \frac{k}{F_y} \dot{u} \left[1 - |z|^n (\beta \operatorname{sgn}(\dot{u}z) + \gamma) \right] \quad (2.2)$$

where β and γ are parameters controlling the shape of the hysteresis, n a parameter that controls the sharpness of the smooth transition from the elastic to the inelastic region of the hysteresis, $\operatorname{sgn}()$ the signum function, and the overdot denotes derivative with respect to time.

Eqn. 2.1 shows that the Bouc-Wen model accounts for kinematic hardening (i.e., post-yield force increases with increasing deformation) due to the post-yield stiffness ratio p . However, the model does not account for the isotropic hardening (i.e., yield force F_y increases due to cyclic inelastic deformation) in the hysteresis of steel energy dissipation devices.

2.1. Mathematical formulation

To incorporate isotropic hardening in the Bouc-Wen model, the yield force F_y needs to be updated by considering the history of the imposed cyclic deformation u . Examination of the constitutive Eqns. 2.1 and 2.2 reveals that a change in the yield force F_y can be achieved by appropriately including a third shape control parameter Φ in Eqn. 2.2:

$$\dot{z} = \frac{k}{F_y} \dot{u} \left[1 - |z|^n (\beta \operatorname{sgn}(\dot{u}z) + \gamma - \Phi \operatorname{sgn}(\dot{u})(\operatorname{sgn}(z) + \operatorname{sgn}(\dot{u}))) \right] \quad (2.3)$$

The parameter Φ quantifies isotropic hardening and is calculated using functions that cause Φ to increase exponentially with increasing cumulative plastic deformation $u_{pl,c}$, i.e.,

$$\Phi_p = \Phi_{\max,p} \left[1 - \exp \left(-p_{\Phi,p} \left| \frac{u_{pl,c}}{u_y} \right| \right) \right] \quad (2.4.a)$$

or

$$\Phi_n = \Phi_{\max,n} \left[1 - \exp \left(-p_{\Phi,n} \left| \frac{u_{pl,c}}{u_y} \right| \right) \right] \quad (2.4.b)$$

where $u_y (=F_y/k)$ is the yield deformation, $p_{\Phi,p}$ and $p_{\Phi,n}$ parameters that control the isotropic hardening rate due to cumulative plastic deformation, and, $\Phi_{\max,p}$ and $\Phi_{\max,n}$ the maximum possible values of Φ for the fully saturated isotropic hardening condition, i.e., for $u_{pl,c} \rightarrow \infty$, $\Phi_p \rightarrow \Phi_{\max,p}$ and $\Phi_n \rightarrow \Phi_{\max,n}$. On the other hand, when $u_{pl,c}=0.0$, $\Phi_p=0.0$ and $\Phi_n=0.0$.

Φ_p and Φ_n are used to independently capture isotropic hardening in different loading directions (positive and negative). Typically, yielding devices exhibit the same isotropic hardening in different loading directions, and therefore, $\Phi_{\max,p}=\Phi_{\max,n}$ and $p_{\Phi,p}=p_{\Phi,n}$. However, the model can simulate

different isotropic hardening in different loading directions (e.g., compressive and tensile loading in BRB hysteresis (Merritt et al. 2003) by using different parameter values in Eqns. 2.4.a and 2.4.b.

To understand the effect of Φ , consider the proposed Bouc-Wen model with $p=0.0$ (i.e., without kinematic hardening), $n=1$ and $\beta+\gamma=1$, under a positive deformation increment, i.e., $\text{sgn}(\dot{u})=1$. Assume that in the previous deformation increment, z has reached its positive ultimate value z_u , and therefore, $\text{sgn}(z)=1$ and $\dot{z}=0.0$. For this case, Eqn. 2.3 yields $z_u=1/(1-2\cdot\Phi)$ and Eqn. 2.1 yields $F=F_y\cdot z_u=F_y/(1-2\cdot\Phi)$. When $\Phi=0.0$ (i.e., without isotropic hardening), F is equal to $F_y/(1-0.0)=F_y$. When $\Phi\neq 0.0$ (e.g., $\Phi=0.1$), F is equal to $F_y/(1-2\cdot\Phi)=F_y/(1-2\cdot 0.1)=1.25\cdot F_y$. In that case, Φ reflects a 25% percent increase in the initial yield strength F_y due to isotropic hardening. The term $\text{sgn}(\dot{u})$ after the parameter Φ in Eqn. 2.3 ensures that the above calculations apply to the case of a negative deformation increment and a negative ultimate value of z .

The state determination procedure of the model requires as an input the previous force and deformation, the previous z value and the current deformation. The current value of the parameter Φ is then calculated based on the following rules: Eqn. 2.4.a is used to update Φ_p when the deformation increment changes from negative to positive within the plastic region of the hysteresis; Eqn. 2.4.b is used to update Φ_n when the deformation increment changes from positive to negative within the plastic region of the hysteresis; Φ equals to Φ_p when a positive deformation increment occurs; and Φ equals to Φ_n when a negative deformation increment occurs. With the current Φ value known, Eqn. 2.3 is numerically integrated to obtain the current value of z which is used in Eqn. 2.1 to provide the current force output F of the model.

The state determination procedure is verified using the following model parameters: $F_y = 220\text{kN}$, $k=440\text{ kN/mm}$, $u_y = F_y/k = 0.5\text{ mm}$, $p = 0.0047$, $\beta = 0.59$, $\gamma = 0.41$, $n = 1$, $\Phi_{\max,p} = \Phi_{\max,n} = 0.2844$ and $p_{\Phi,p} = p_{\Phi,n} = 0.0135$. The imposed cyclic deformation history u (in mm) is: $0.0 \rightarrow +6.0 \rightarrow -6.0 \rightarrow +9.5$. Figures 1.a and 1.b show the $z-u$ and $F-u$ hysteresis from state determination along with numerical integration of Eqn. 2.3 using a Newton-Raphson scheme. The plastic deformations ($u_{pl,1}$ and $u_{pl,2}$ in Fig. 2.1.b) are calculated with respect to the yielding deformations $u_{y,1}^*$ ($=u_y=0.5\text{ mm}$) and $u_{y,2}^*$ ($=4.9\text{ mm}$) where the extrapolated lines of the elastic and the plastic region of the $F-u$ hysteresis meet. To verify the hysteresis in Figs. 2.1.a and 2.1.b, Eqn. 2.3 is analytically solved for the different cases shown in Fig. 2.1.a as follows:

Case 1 with $z>0$ and $\dot{u} >0$ (points 1 to 2): $\Phi=\Phi_p=0.0$; the initial conditions are $u_{init}=0.0\text{ mm}$ and $z_{init}=0.0$; the analytical solution of Eqn. 2.3 is $z(u)=(1/(1-2\cdot\Phi))\cdot(1-\exp(-(1-2\cdot\Phi)\cdot(u-u_{init})/u_y))$; and $z(6)=1.0$.

Case 2 with $z>0$ and $\dot{u} <0$ (points 2 to 3): $u_{y,1}^*=u_y=0.5\text{ mm}$; $u_{pl,c}=u_{pl,1}=6-0.5=5.5\text{ mm}$; $\Phi=\Phi_n=0.0392$; the initial conditions are $u_{init}=6\text{ mm}$ and $z_{init}=1.0$; the analytical solution of Eqn. 2.3 is $z(u)=-5.56+6.56\cdot\exp(0.18\cdot(u-u_{init})/u_y)$; and $z(u)=0.0$ at $u=5.54\text{ mm}$.

Case 3 with $z<0$ and $\dot{u} <0$ (points 3 to 4): $\Phi=\Phi_n=0.0392$; the initial conditions are $u_{init}=5.54\text{ mm}$ and $z_{init}=0.0$; the analytical solution of Eqn. 2.3 is $z(u)=(1/(1-2\cdot\Phi))\cdot(-1+\exp((1-2\cdot\Phi)\cdot(u-u_{init})/u_y))$; and $z(-6)=-1.09$.

Case 4 with $z<0$ and $\dot{u} >0$ (points 4 to 5): $u_{y,2}^*=4.9\text{ mm}$; $u_{pl,c}=u_{pl,1}+u_{pl,2}=5.5+(4.9+6)=16.4\text{ mm}$; $\Phi=\Phi_p=0.1017$; the initial conditions are $u_{init}=-6\text{ mm}$ and $z_{init}=-1.09$; the analytical solution of Eqn. 2.3 is $z(u)=5.56-6.65\cdot\exp(-0.18\cdot(u-u_{init})/u_y)$; and $z(u)=0.0$ at $u=-5.5\text{ mm}$.

Case 5 with $z>0$ and $\dot{u} >0$ (points 5 to 6): $\Phi=\Phi_p=0.1017$; the initial conditions are $u_{init}=-5.5\text{ mm}$ and $z_{init}=0.0$; the analytical solution of Eqn. 2.3 is the same with that of Case 1; and $z(9.5)=1.26$

The above analytical solutions can be used to verify the $z-u$ and $F-u$ hysteresis. As an example, consider point A in Figs. 2.1.a and 2.1.b. Inputting $u=-5.8\text{ mm}$ in the analytical $z(u)$ solution for Case 4 gives $z(-5.8)=-0.63$, and hence, Eqn. 2.1 gives $F=-149\text{ kN}$ for $u=-5.8$ and $z=-0.63$.

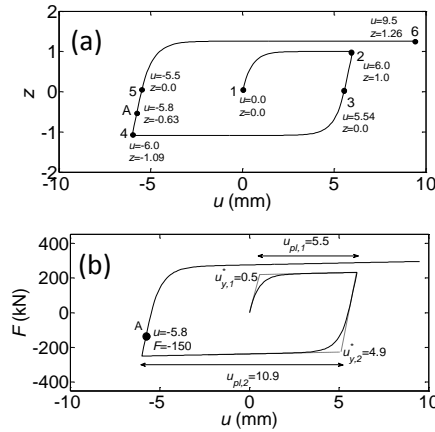


Figure 2.1. (a) Analytical verification of the z - u ; and (b) F - u hysteresis of the proposed model under cyclic deformation.

2.2. Model calibration against experimental results

The parameters of the model are determined from characterization test data on steel yielding devices available in literature. An unconstrained nonlinear minimization method is used to minimize the root mean square error (RMS)

$$RMS = \sqrt{\frac{\sum_{i=1}^N (F_i - F_{exp i})^2}{\sum_{i=1}^N F_i^2}} \quad (2.5)$$

where N is the number of the available experimental force (F_{exp}) data points and F is the force of the model (see Eqn. 2.1). Fig. 2.2 shows test data and results from the proposed hysteretic model for slit steel devices (Chan and Albermani 2008), low-yield steel shear panels exhibiting significant isotropic hardening (Nakashima 1995) and BRBs exhibiting different isotropic hardening in tension and compression (Merritt et al. 2003). Table 2.1 provides information for the test specimens and the model parameters as well as the RMS values which indicate the accuracy of the proposed model.

Table 2.1. Model parameters calibrated from experimental results

Spec.	F_y (kN)	k (kN/m)	p	β	γ	n	Φ_{max}	p_{Φ}	RMS
SL-3	19	10	0.04	0.90	0.10	1.0	0.11	0.013	0.07
SP-9	225	442	0.005	0.56	0.44	1.0	0.28	0.0135	0.08
BRB	1050	94	0.017	0.84	0.16	1.0	0.15*	0.1**	0.13

*0.20 and **0.15: values of parameters for Eqn. 3: different isotropic hardening in tension and compression

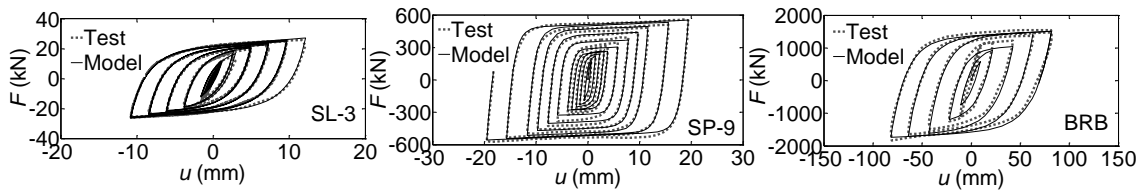


Figure 2.2. Test data and results from the proposed model for slit steel devices (left); low-yield shear panels (centre); and BRBs (right).

2.3. Design of slit steel devices

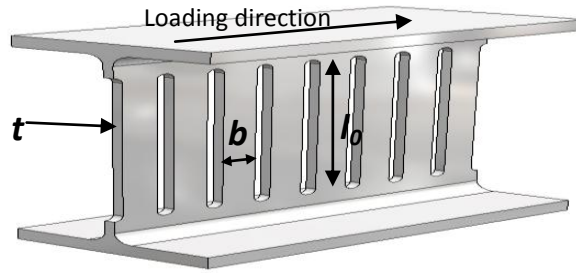


Figure 2.3. Slit steel device

Chan and Albermani (2008) designed and tested steel devices fabricated from a short length of an I section with a number of slits cut from the web, leaving a number of strips between the two flanges to deform in flexure and dissipate energy by forming plastic hinges at their ends. As shown in Fig. 2.3, the variables involved in the design of the device are the strip length l_0 , strip depth b and web thickness t .

The yield strength P_y of the device is equal to

$$P_y = c_y \frac{n_{st} \sigma_y t b^2}{2l_0} \quad (2.6)$$

where n_{st} is the number of strips in the device, σ_y is the yield strength of the material and c_y is a correction factor to be determined by experimental results. In addition, the elastic stiffness k_e of the device is calculated through

$$k_e = c_k \frac{n_{st} E t b^3}{l_0^3} \quad (2.7)$$

where E is the Young's modulus and c_k is a stiffness correction factor to be determined by experimental results.

Based on the calibrated values of the stiffness k and F_y of the proposed model and the properties of all the slit steel devices tested in (Chan and Albermani 2008), the mean values of the corrections factor c_y and c_k were found equal to 1.45 and 0.22, respectively. Eqn. 2.6 provides the force level at which the device yields. However, the ultimate strength, F_u , of the device is needed in order to enable reliable capacity design of the main structural members of the frame (beams, columns and braces). The mean value of the ratio of the ultimate device strength to the yield strength, i.e., F_u/F_y , was found equal to 1.32. Another design parameter is the ultimate cyclic deformation capacity u_{ult} before fracture. Based on the tests presented in (Chan and Albermani), u_{ult} can be conservatively considered equal to $35u_y$.

3. MINIMAL-DAMAGE STEEL BUILDING WITH STEEL YIELDING DEVICES AND VISCOUS DAMPERS

3.1. Prototype building

Fig. 3.1 (left) shows the plan view of the 5-story, 3-bay by 3-bay prototype office building used for the study. The building has two 3-bay perimeter steel MRFs (one at each side) to resist lateral forces in the

N-S direction. The design study focuses on one perimeter MRF. This MRF is designed either as a conventional MRF or as an MRF with steel slit devices and viscous dampers in order to compare their seismic response. The slit devices are supported by braces and connected to the bottom flange of the beam of the steel MRF. The viscous dampers are inserted in an interior gravity frame (with pin connections) of the building. The MRF with slit devices and the gravity frame with viscous dampers are coupled due to the floor diaphragm and form a hybrid lateral-load resisting system, referred to herein as the steel MRF with slit devices and viscous dampers, which is shown in Fig. 3.1 (right). The yield stress of structural steel is assumed to be equal to 275 MPa. The design Type 1 response spectrum of the EC8 with a peak ground acceleration of 0.3g and ground type B represents the DBE.

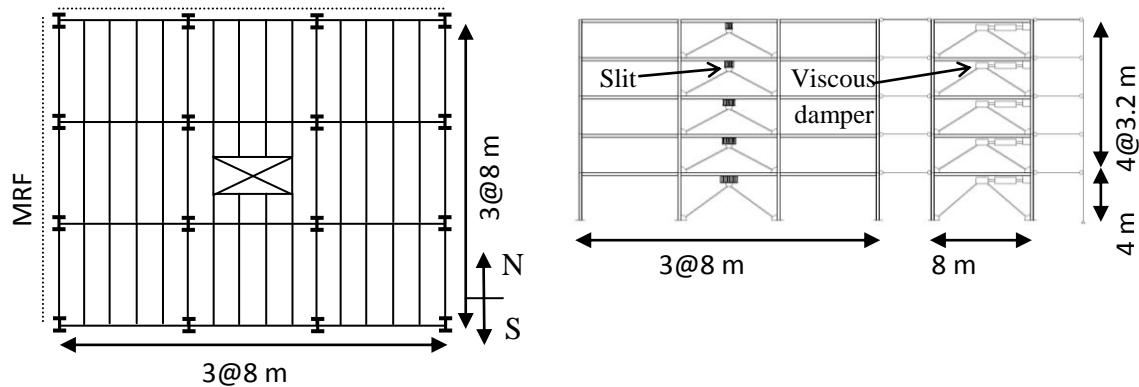


Figure 3.1 Prototype building structure: plan view (left); perimeter steel MRF with slit steel devices and interior gravity frame with viscous dampers (right).

3.2. Design of conventional steel MRF

The perimeter MRF of the building is designed as a conventional steel MRF according to EC3 and EC8. The behavior (or “strength reduction”) factor q is equal to 6.5. The displacement behaviour factor (equal to q) is used to estimate peak inelastic drifts. A 0.75% serviceability limit on the peak story drift, θ_{\max} , under the frequently occurred earthquake (FOE) with intensity equal to 40% of the intensity of the DBE is adopted.

3.3. Design of steel MRF with slit devices and viscous dampers

3.3.1. Minimal-damage-based performance objectives

Immediate occupancy (IO) under the DBE: According to EC8, drift-sensitive non-structural elements designed not to interfere with structural deformations can avoid damage for $\theta_{\max}=1\%$. There is no consensus for defining a residual story drift, θ_r , target value associated with IO. The target θ_r is set equal to the global sway imperfections defined in EC3, equal to 0.264% for the geometry of the prototype building in Fig. 3.1. Based on the results presented in (Karavasilis and Seo 2011), the residual storey drift of the steel MRF with slit devices and viscous dampers is conservatively estimated equal to 0.15% of θ_{\max} , i.e., $\theta_r=0.15 \cdot 1\%=0.15\%$ which is lower than the target 0.264% value and can be easily straightened in the aftermath of the DBE by replacing damaged slit devices. In addition, beams and columns of the MRF can be damage-free for $\theta_{\max}=1.0\%$.

Rapid return to occupancy under the MCE: The MCE has intensity 150% the intensity of the DBE, and hence, $\theta_{\max}=1.5 \cdot 1\%=1.5\%$. Main structural members can be designed to behave elastically for $\theta_{\max}=1.5\%$ (Karavasilis et al. 2011). However, drift-sensitive non-structural elements will sustain controlled damage which should be repaired for $\theta_{\max}=1.5\%$. The residual storey drift is estimated equal to $\theta_r=0.15 \cdot 1.5\%=0.225\%$ (Karavasilis and Seo 2011). This value is lower than the previously defined target θ_r value associated with IO (i.e., 0.264%) and can be straightened by replacing damaged slit devices.

Peak total floor accelerations should also be controlled to avoid having toppled or dropped non-structural elements and dysfunctional acceleration-sensitive equipment. The results presented in (Karavasilis and Seo 2011) showed that drifts and total accelerations can be simultaneously controlled by providing supplemental damping to systems with low strength. Therefore, the steel MRF with slit devices should be designed for low strength, and then, viscous dampers should be designed to reduce drifts at the target θ_{\max} , equal to 1.0% under the DBE.

3.3.2. Design procedure

The q factor is equal to 6.5 and defines the force level at which slit devices are expected to yield. The slit devices dimensions are selected based on Eqns 2.6 and 2.7 in order to provide the required stiffness and strength. In addition, the required slit device fracture capacity is checked. Beams, columns and braces are designed to avoid yielding and buckling under the ultimate slit devices forces using standard capacity design rules. Under the DBE, the MRF with slit devices has $\theta_{\max}=1.5\%$. Nonlinear viscous dampers are designed to provide a supplemental viscous damping ratio ξ_s equal to 18% according to

$$\xi_s = \frac{\sum_j (2\pi)^a T^{2-a} \lambda_j c_j u_r^{a-1} (\phi_j - \phi_{j-1})^{1+a}}{8\pi^3 \sum_j m_i \varphi_j^2} \quad (3.1)$$

where j denotes a specific story of the MRF, a is the velocity exponent of the nonlinear viscous dampers (equal to 0.5), T the fundamental period of vibration, λ a dimensionless parameter, c the damper constant, u_r the amplitude of the roof displacement, m the story mass, and φ the coordinate of the first mode shape (Whittaker et al. 2003). Adding 18% damping to the inherent 2% damping of the MRF provides a response spectrum damping reduction factor equal to 1.5 (Whittaker et al. 2003) and hence, the θ_{\max} under the DBE is reduced to $1.5\%/1.5=1.0\%$, i.e., equal to the target peak story drift value (Section 3.3.1).

3.3.3 Design details

Table 3.1. Properties of conventional and proposed steel MRFs

St.	Conventional MRF					MRF with slit dev. and damp.				
	Col. (HEB)	Beam (IPE)	T (s.)	Steel (kN)	θ_{\max} (%)	Col. (HEB)	Beam (IPE)	T (s.)	Steel (kN)	θ_{\max} (%)
1	400	450			DBE	280	270			DBE
2	400	450	1.7	180	1.75	280	270	1.5	124	1.0
3	400	400				280	270			
4	360	400			MCE	240	240			MCE
5	360	360			2.63	240	240			1.5

Table 3.2. Slit devices and viscous dampers properties

St.	Damper constant c {kN(s./mm) ^{0.5} }	Slit device geometry $t/b/l_o$ (mm)	Slit device number of strips n_{st}
1	33.2	15/66/440	13
2	38.0	15/53/350	15
3	34.0	15/53/350	13
4	25.1	15/53/350	10
5	19.1	15/53/350	8

Table 3.1. provides design details for the conventional MRF and the MRF with slit devices and viscous dampers and shows the significant benefits (lower θ_{max} and reduced steel weight) offered by the proposed seismic design strategy. In addition, Table 3.2 shows that slit devices and nonlinear viscous dampers have cost-effective practical sizes.

4. Nonlinear dynamic analyses

The proposed model for steel yielding devices is implemented in OpenSees and used to model slit devices. Nonlinear viscous dampers are modeled to have a force output f_d

$$f_d = c|v|^a \text{sgn}(v) \quad (4.1)$$

where v is the velocity across the damper. A fiber beam column is used to model beams, columns and braces, while nonlinear rotational springs are used to model panel zones. Twenty ground motions scaled to the DBE and MCE level were used for dynamic analysis (Karavasilis et al. 2011).

Fig. 4.1 (top) compares the roof drift time histories of the conventional steel MRF and the MRF with slit devices and viscous dampers under a ground motion scaled to the DBE. The MRF with slit devices and viscous dampers shows negligible residual drift. Fig. 4.1 (bottom) shows the slit device and nonlinear viscous damper hysteresis in the third storey of the building.

Fig. 4.2 shows statistics of θ_{max} , θ_r and peak total floor accelerations a_{max} from nonlinear dynamic analyses. The results indicate significantly higher performance of the MRF with dampers compared to the conventional MRF. In addition, the values of θ_{max} and θ_r are very close to the design target values (Section 3.3.1) and confirm that the proposed MRF achieves IO under the DBE and RRO under the MCE.

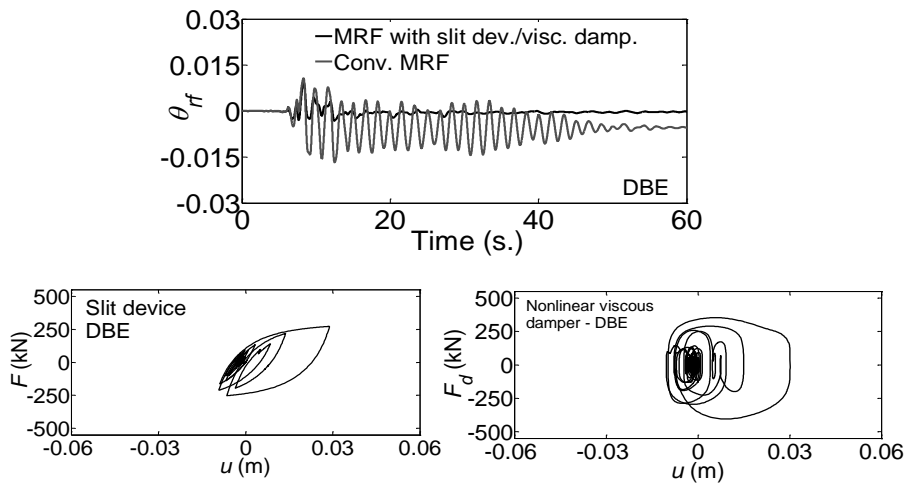


Figure 4.1 . Comparison of roof drift time histories (top); and, slit device and viscous damper hysteresis in the third storey of the minimal-damage steel MRF (bottom) under a ground motion scaled to the DBE

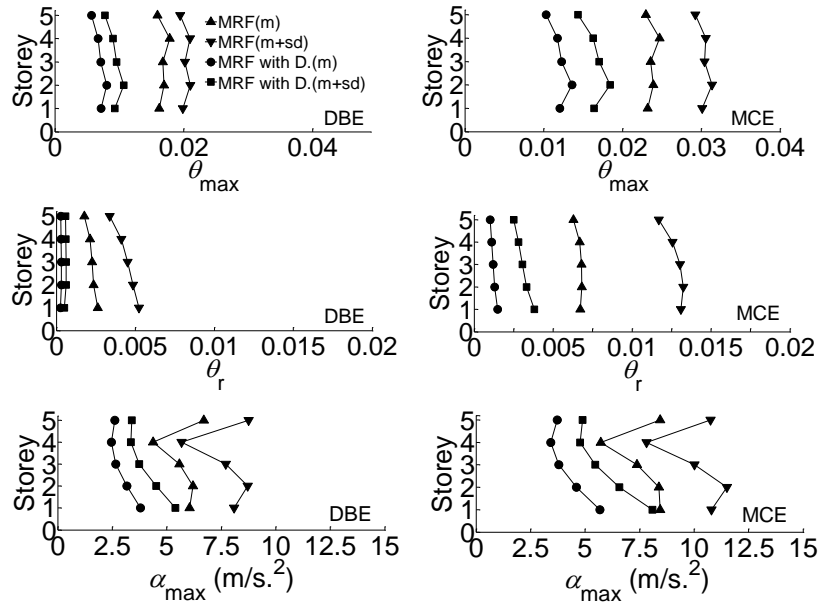


Figure 4.2. Statistics of peak story drifts, residual story drifts and peak total accelerations of the conventional MRF and the MRF with slit devices and viscous dampers

5. SUMMARY AND CONCLUSIONS

A model for steel energy dissipation devices was developed and calibrated against existing experimental results. A simplified seismic design procedure was proposed and used to design a prototype steel building equipped with steel devices and viscous dampers according to explicitly defined minimal-damage performance objectives. The same building was designed as a conventional steel MRF according to EC8. Based on the results presented in this paper, the following conclusions are drawn:

- The versatile Bouc-Wen model can be modified to capture the combined kinematic and isotropic hardening seen in the hysteresis of steel energy dissipation devices. The model is able to predict the hysteresis of slit devices, low-yield steel shear panels and buckling-restrained braces.
- The proposed seismic design procedure for steel buildings equipped with steel devices and rate-dependent dampers was confirmed with nonlinear dynamic analyses.
- Seismic analyses indicated that the building with slit devices and nonlinear viscous dampers achieves immediate occupancy under the design earthquake and rapid return to occupancy under the maximum considered earthquake by avoiding yielding in main structural members and by satisfying target peak storey drift and residual storey drift values.
- Residual storey drifts of the conventional MRF did not satisfy the critical 0.5% value which ensures reparability based on findings from past earthquakes.
- Total floor accelerations can be reduced while achieving significant drift reductions by designing a structure to have reduced strength and supplemental viscous damping.

ACKNOWLEDGEMENT

Acknowledgement heading is to be typed using Times New Roman 10 pt bold and with all caps, but not numbered. Text of the acknowledgement should be typed using Times New Roman 10 pt regular and justified. No blank line should be left between the heading and the text. Leave two blank lines after the text 10 pt size.

REFERENCES

CEN. 2004. Eurocode 8: design of structures for earthquake resistance. Part 1: General rules, seismic actions and rules for buildings.

- Chan, R.-W.K., Albermani, F. (2008). Experimental study of steel slit damper for passive energy dissipation. *Engin. Structures* **30**,1058-1066.
- Nakashima, M. (1995). Strain-hardening behavior of shear panels made of low-yield steel. I: Test. *J. of Struct. Engin.* **121:12**, 1742-1749.
- Meritt, S., Uang, C.M. and Benzoni, G. (2003). Subassemblage testing of star seismic buckling-restrained braces. Structural Systems Research Project, Report No. TR-2003/04, University of California, San Diego.
- Wen, Y.K. (1976). Method for random vibration of hysteretic systems. *J. of Eng. Mech Division.* **102:2**,249-263.
- Mazzoni, S., McKenna, F., Scott, M. and Fenves, G. (2006). OpenSees. User Command Language Manual. PEER Center, University of California, Berkeley.
- CEN. 2005. Eurocode 3: design of steel structures. Part 1-1: General rules and rules for buildings.
- Karavasilis, T.L. and Seo, C.Y. (2011). Seismic structural and non-structural performance evaluation of highly damped self-centering and conventional systems. *Engin. Struct.* **33**,2248-2258.
- McCormick, J., Aburano, H., Ikenaga, M. and Nakashima, M. (2008). Permissible residual deformation levels for building structures considering both safety and human elements. *14th WCEE, Beijing, China.*
- Whittaker, A.S., Constantinou, M.C., Ramirez, O.M., Johnson, M.W. and Chrysostomou, C.Z. (2003). Equivalent lateral force and modal analysis procedures of the 2000 NEHRP Provisions for buildings with damping systems. *Earthq. Spectra.* **19:4**,959-980.
- Karavasilis, T.L., Kerawala, S. and Hale, E. (2012). Hysteretic model for steel energy dissipation devices and evaluation of a minimal-damage seismic design approach for steel buildings. *J. of Constr. Steel Research.* **70**:358-367.